

# Momentum-Transfer to and Elementary-Excitations of a Bose-Einstein Condensate by a Time-Dependent Optical Potential

Y. B. Band and M. Sokuler

*Departments of Chemistry and Physics, Ben-Gurion University of the Negev, Beer-Sheva, Israel 84105*

We present results of calculations on Bose-Einstein condensed  $^{87}\text{Rb}$  atoms subjected to a moving standing-wave light-potential of the form  $V_L(z, t) = V_0(t) \cos(qz - \omega t)$ . We calculate the mean-field dynamics (the order parameter) of the condensate and determine the resulting condensate momentum in the  $z$  direction,  $P_z(q, \omega, V_0, t_p)$ , where  $V_0$  is the peak optical potential strength and  $t_p$  is the pulse duration. Although the local density approximation for the Bogoliubov excitation spectral distribution is a good approximation for very low optical intensities, long pulse duration and sufficiently large values of the wavevector  $q$  of the light-potential, for small  $q$ , short duration pulses, or for not-so-low intensities, the local density perturbative description of the excitation spectrum breaks down badly, as shown by our results.

## I. INTRODUCTION

Elementary excitations of a Bose-Einstein condensate (BEC) can be explored with matter-wave interference studies using two-photon Bragg pulse spectroscopy [1–10]. In such studies, the momentum imparted to the BEC by a Raman scattering process can be studied as a function of the temporal duration of the optical pulses,  $t_p$ , the detuning of the Bragg pulses from atomic resonance,  $\Delta$ , the intensity of the Bragg pulses, the difference of the Bragg pulse wavevectors which is denoted by the wavevector  $\mathbf{q}$ , and the difference of the central frequency of the two laser pulses  $\omega$ . In the linear response limit, the response of the BEC to a weak perturbation with wavevector  $\mathbf{q}$  and energy  $\hbar\omega$  is given in terms of the dynamic structure factor  $S(\mathbf{q}, \omega)$  [11],

$$S(\mathbf{q}, \omega) = \frac{1}{\mathcal{Z}} \sum_{m,n} e^{-\beta E_m} |\langle m | \delta\rho_{\mathbf{q}} | n \rangle|^2 \delta(\omega - \omega_{mn}), \quad (1)$$

where  $\beta = 1/kT$ ,  $\hbar\omega_{mn} = E_m - E_n$  is the difference of two energy eigenvalues of the BEC, the density fluctuation  $\delta\rho_{\mathbf{q}}$  is induced by a perturbation with wavevector  $\mathbf{q}$  and frequency  $\omega$  that oscillates like  $e^{i(\mathbf{q}\cdot\mathbf{r} - \omega t)}$ , and  $\mathcal{Z}$  is the usual partition function. The momentum imparted to the BEC by the light-potential and its dependence on the wavevector  $\mathbf{q}$  and frequency  $\omega$  can be directly related to the structure factor  $S(\mathbf{q}, \omega)$ , and to the Bogoliubov dispersion relation,  $E_B(\mathbf{q})$  versus  $\mathbf{q}$  [12]. The excitation modes of a BEC have been measured [13,14] and can be directly related to  $S(\mathbf{q}, \omega)$  and  $E_B(\mathbf{q})$ . The momentum transferred to a BEC by a moving standing-wave light-potential has also been directly measured over a wide range of  $\mathbf{q}$  and  $\omega$  [7,9,10], and it is of interest to calculate the momentum transfer versus  $\mathbf{q}$  and  $\omega$  so that the calculations can be compared with experiment.

Here we report on the results of calculations of BEC excitation by Bragg pulse spectroscopic techniques to obtain the momentum transfer versus  $\mathbf{q}$  and  $\omega$  for weak and strong optical excitations. We find that, even with what is ordinarily considered weak intensity Bragg pulses, processes that are higher than first order (linear response) play a role in the excitation process. We also find that a local density Bogoliubov description is not valid for small wavevectors  $q$ . We describe the nature of the higher order processes and their influence on the momentum and energy of the BEC excitation. We show how the simple Bogoliubov picture of the excitation is modified over a range of momentum-transfers and excitation energies due to higher order light-scattering processes, finite BEC size and inhomogeneity effects.

We consider Bose-Einstein condensed  $^{87}\text{Rb}$  atoms in the  $|F = 2, M_F = 2\rangle$  hyperfine state confined in a harmonic oscillator potential, an array of optical traps and a gravitational field, and use parameters similar to those used in experiments carried out at the Weizmann Institute [10]. The initial BEC is cigar shaped with  $N = 10^5$  atoms in a static harmonic trap potential  $V_{ho}(\mathbf{r}) = \frac{m\omega_z^2}{2}z^2 + \frac{m\omega_{x,y}^2}{2}(x^2 + y^2)$  with frequencies  $\omega_z = 2\pi \times 25$  Hz,  $\omega_{x,y} \equiv \omega_x = \omega_y = 2\pi \times 220$  Hz ( $\bar{\omega} \equiv (\omega_x\omega_y\omega_z)^{1/3} = 2\pi \times 106$  Hz). The Bragg pulses propagate with wavevectors  $\mathbf{k}_1$  and  $\mathbf{k}_2$  in the  $x$ - $z$  plane with angles  $\pm\theta/2$  relative to the  $x$  axis. The central frequency of one pulse is greater than that of the other,  $\omega_2 = \omega_1 - \omega$ , and the difference frequency  $\omega$  is controlled using an acousto-optic modulator. The electric field takes the form  $\mathbf{E}(t) = \mathbf{E}_1(t) \exp[i(\mathbf{k}_1 \cdot \mathbf{x} - \omega_1 t)] + \mathbf{E}_2(t) \exp[i(\mathbf{k}_2 \cdot \mathbf{x} - \omega_2 t)]$ , with lin || lin configuration for the field polarizations and equal

intensities for the two Bragg pulses. When the Bragg pulses are switched on, the atoms are trapped at the antinodes of a vertically oriented, red-detuned optical moving standing-wave; the antinodes are separated by  $\Delta z = \lambda/(2 \sin(\theta/2))$ . The momentum transferred to an atom upon absorbing a photon from the field with wavevector  $\mathbf{k}_1$  and emitting a photon with wavevector  $\mathbf{k}_2$  is given by  $\hbar\mathbf{q} = \hbar(\mathbf{k}_1 - \mathbf{k}_2) = \hbar q \hat{z}$ , where the  $\hbar q = 2\hbar k_{ph} \sin(\theta/2)$ , and  $\hbar k_{ph} = 2\pi\hbar/\lambda$  is the photon momentum. Here  $\lambda = 780$  nm is the central wavelength of the Bragg pulses. The light-potential experienced by the atoms in the BEC as a result of the Bragg pulses is given by  $V_L(z, t) = V_0(t) \cos(qz - \omega t)$ . The well-depth of the optical potential,  $V_0(t)$ , is proportional to the intensity of the Bragg pulses and inversely proportional to the detuning from resonance,  $\Delta$ , i.e.,  $V_0(t) = \frac{\hbar\Omega_1(t)\Omega_2(t)}{4\Delta}$  where  $\Omega_1(t)$  and  $\Omega_2(t)$  are the Rabi frequencies. The well-depth temporal dependence  $f(t)$ , where  $V_0(t) = V_0 f(t)$ , is taken to have a Gaussian rise-time and fall-time of width  $t_r = 20 \mu\text{s}$ ;  $V_0(t)$  is constant for a time duration  $t_p$  between the rise and fall ( $f(t) = 1$  for the time interval  $t_p$  so  $V_0(t) = V_0$  in this interval). Pulses with short ( $t_p = 1$  ms) and long pulse duration ( $t_p = 6$  ms) are used. The strength of  $V_0$  that is used in the calculations will be specified in recoil units,  $E_R \equiv (\hbar k_{ph})^2/(2m)$ . Absorption of a photon from one pulse and stimulated emission into the other pulse produces a perturbation with energy  $\hbar\omega$  and momentum  $\hbar q \hat{z}$ . In the experiments, the light-potential and the harmonic potential are both switched-off (dropped), releasing the atoms to fall under the influence of gravity, and absorption images are taken after the particles evolve for some specified period of time under the influence of gravity.

## II. THEORETICAL FORMULATION

We calculate the dynamics within a mean-field treatment using the time-dependent Gross-Pitaevskii equation (GPE) [15,16],

$$i\hbar \frac{\partial \psi(\mathbf{r}, t)}{\partial t} = \left( \frac{p^2}{2m} + V(\mathbf{r}, t) + g|\psi|^2 \right) \psi, \quad (2)$$

where

$$V(\mathbf{r}, t) = V_{ho}(\mathbf{r}) - mgz + V_L(z, t), \quad (3)$$

is the potential, and  $g = \frac{4\pi N a_0 \hbar^2}{m}$  is the atom-atom nonlinear interaction strength which is proportional to the  $s$ -wave scattering length  $a_0$  and the total number of condensed atoms  $N$ . The wave function (order parameter)  $\psi(\mathbf{r}, t)$  is propagated with a split-operator fast Fourier transform method. Due to the large number of grid points necessary in the lattice direction ( $z$ ), we found it necessary to convert the 3D GPE into an effective 1D GPE with similar dynamics as described in Ref. [17]. The wave function in momentum space,  $\psi(k_z, t)$ , is determined by taking the Fourier transform of  $\psi(z, t)$ . The net momentum of the BEC at any time  $t$  is given by

$$P_z(t) = \int_{-\infty}^{\infty} dk_z \psi^*(k_z, t) (\hbar k_z) \psi(k_z, t). \quad (4)$$

The expectation values of all dynamical quantities (e.g., energies,  $\langle \Delta z \rangle$ , etc.) can be easily determined using the calculated wavepackets in either position or momentum space.

A perturbative estimate of the rate of momentum-transfer to the BEC by the Bragg pulses is given by [18]

$$\frac{dP_z(t)}{dt} = \frac{2\pi}{\hbar} q \left( \frac{V_0}{2} \right)^2 [S(\mathbf{q}, \omega) - S(-\mathbf{q}, -\omega)]. \quad (5)$$

For a uniform zero-temperature BEC, the Bogoliubov excitation energy at momentum-transfer  $\mathbf{q}$  is

$$E_B(q) \equiv \hbar\Omega_B(q) = \sqrt{\epsilon(q)[\epsilon(q) + 2gn]}, \quad (6)$$

where  $\epsilon(q) = (\hbar q)^2/2m$ ,  $n$  is the density, and the dynamic structure factor is given by  $S(\mathbf{q}, \omega) = \frac{\epsilon(q)}{E_B(q)} \delta(\hbar\omega - E_B(q))$ . Hence, the momentum transferred is given by

$$P_z(t) = \frac{\pi}{2\hbar} \left( \int_0^t dt' V_0^2(t') \right) \frac{q\epsilon(q)}{\sqrt{\epsilon(q)[\epsilon(q) + 2gn]}} \delta(\hbar\omega - E_B(q)). \quad (7)$$

Thus, the momentum transferred by a moving standing-wave excitation to a uniform condensate is non-vanishing only when  $\omega = \Omega_B(q)$ , and its magnitude is proportional to the product of the integral over time of  $V_0^2$  and  $\frac{q\epsilon(q)}{E_B(q)}$ .

For a non-uniform BEC with density profile that varies smoothly with position, one can define a local Bogoliubov excitation energy,

$$E_B(q, \mathbf{r}) \equiv \hbar\Omega_B(q, \mathbf{r}) = \sqrt{\epsilon(q)[\epsilon(q) + 2gn(\mathbf{r})]}, \quad (8)$$

and a local density approximation dynamic structure factor that behaves locally as a uniform gas [7]:

$$S_{LDA}(\mathbf{q}, \omega) = N^{-1} \int d\mathbf{r} n(\mathbf{r}) \frac{\epsilon(q)}{E_B(q, \mathbf{r})} \delta(\hbar\omega - E_B(q, \mathbf{r})). \quad (9)$$

Hence, in perturbation theory (i.e., small  $V_0$ ), the momentum transferred to the non-uniform condensate can be approximated by substituting  $S_{LDA}(\mathbf{q}, \omega)$  for  $S(\mathbf{q}, \omega)$  on the right hand side of Eq. (5). Thus, momentum transfer of a non-uniform condensate via a moving standing-wave excitation is smeared over a range of frequencies around  $\omega = \Omega_B(q)$ , and its magnitude is determined by carrying out an average of  $\frac{q\epsilon(q)}{E_B(q, \mathbf{r})}$  over the local density.

### III. RESULTS

Calculations were carried out over a range of momentum-transfer  $q$  (i.e., a range of angles  $\theta$ ), frequencies  $\omega$ , pulse duration times  $t_p$ , and laser pulse intensities (potential strengths  $V_0$ ).

Fig. 1 shows the calculated momentum imparted to the BEC by the Bragg pulses,  $P_z(q, \omega, V_0, t_p)$ , as a function of  $\omega$  for  $\theta = 22.5^\circ$  ( $q = 0.390 \hbar k_{ph} = 80\sqrt{\hbar m \omega_z}$ ) and pulse duration  $t_p = 6$  ms. The calculations were performed for three different laser intensities corresponding to potential well depths  $V_0 = 0.0054, 0.0162$  and  $0.054 E_R$ . The low intensity curve peaks near the Bogoliubov frequency  $\Omega_B(q) = 8657 \text{ s}^{-1}$ . This peak has a tail at lower  $\omega$  which is due to the non-uniform density of the BEC;  $E_B(q, \mathbf{r})$  for positions away from the center of the BEC is smaller than at the center and this can give rise to the tail, as can be understood from Eqs. (9) and (5). At intermediate and high  $V_0$ , a power broadening of the spectral distribution  $P_z(\omega)$  is evident in Fig. 1; at these values of  $V_0$ , higher order (nonlinear) processes that populate  $\pm 2q$  momenta take place (see Fig. 2). These phenomena can not be understood from a perturbative treatment. At even higher values of  $V_0$ , the spectral distribution becomes even wider and the peak structure becomes even more complicated and ragged.

Fig. 2 shows  $|\psi(k_z, t)|^2$  vs.  $k_z$  for the low intensity case appearing in Fig. 1 for  $\omega = 8945$  and  $9597 \text{ s}^{-1}$ . The net positive momentum, ( $P_z(\omega) > 0$ ) resulting at these frequencies in Fig. 1 is due to the fact that the peak at  $k_z = q$  ( $\approx 0.390 \hbar k_{ph} = 80\sqrt{\hbar m \omega_z}$ ) is larger than that at  $k_z = -q$ . The peak near  $k_z = q$  has an additional high-frequency feature at around  $k_z = 120\sqrt{\hbar m \omega_z}$ ; the origin of this feature is not clearly understood. The peaks at  $k_z = \pm 2q$  are almost two orders of magnitude reduced compared with the  $k_z = \pm q$  peaks. As the intensity of the lasers (the potential well depths) increase, the size of the  $k_z = \pm 2q$  peaks grow in comparison with the  $k_z = \pm q$  peaks, and  $|\psi(k_z, t)|^2$  grows at intermediate values of  $k_z$  between the peaks at  $k_z = \pm jq$ , where  $j$  is a positive integer.

Fig. 3 is similar to Fig. 1, except the pulse duration was taken to be 1 ms. The width of the distribution  $P_z(\omega)$  as a function of  $\omega$  for  $t_p = 1$  ms is considerably wider than for  $t_p = 6$  ms for the low and intermediate intensities. The shorter temporal duration and therefore larger bandwidth of the 1 ms Bragg pulses allows for a wider distribution in frequency of  $P_z(\omega)$  versus  $\omega$ . The width hides the tail of the distribution at lower  $\omega$  due to the non-uniform BEC density. For the high intensity case, the distribution does not change very much from the low and intermediate cases. Moreover, it is narrower than the high intensity 6 ms result shown in Fig. 1 because the pulse fluence is smaller, hence higher order processes do not significantly broaden the distribution. However, for the ultrahigh intensity case, power broadening of the distribution is significant. Note that the perturbation theory expression (5) can not account for the time-domain broadening shown in Fig. 3 (since it is derived assuming that the spectral width of  $V_0$  is within that of  $S(\mathbf{q}, \omega)$ ). Eq. (5) should be modified to account for the bandwidth of the optical pulse:

$$\frac{dP_z(t)}{dt} = \frac{\pi}{2\hbar} q \left( \frac{1}{\sqrt{2\pi}} \int d\omega e^{-i\omega t} |V_0(\omega)|^2 S(\mathbf{q}, \omega) + c.c. \right). \quad (10)$$

This equation should then be integrated over time to obtain an expression that replaces (7) for  $P_z(t)$ .

We now consider smaller values of momentum-transfer  $q$  such that the excitation wavelengths of the optical potential are comparable or larger than the size of the condensate. Fig. 4 shows  $P_z$  versus  $\omega$  for  $\theta = 10^\circ$  ( $q = 0.174 \hbar k_{ph} = 35.8\sqrt{\hbar m \omega_z}$ ) and  $t_p = 6$  ms. The curve for low intensity,  $V_0 = 0.0054 E_R$ , is similar to the low intensity result in Fig. 1 in the sense that a peak exists near the Bogoliubov frequency  $\Omega_B(q) = 4164 \text{ s}^{-1}$  and a low frequency tail is present. Increasing the intensity to  $V_0 = 0.054 E_R$  (the curved labeled high), yields a multi-peaked ragged spectrum due to

higher order nonlinear processes. Upon reducing the optical potential by a factor of 0.3 from the low intensity case to  $V_0 = 0.00162 E_R$  (the curve labeled ultralow), new features in the spectrum become clear. The small feature near  $\omega = 860 \text{ s}^{-1}$  and the tail of the Bogoliubov peak at  $2411 \text{ s}^{-1}$ , which was presumably due to an inhomogeneous density effect, become two ancillary peaks. The reason for the structure in the spectrum for the ultralow (and low) intensity can be understood by looking at  $|\psi(k_z, t)|^2$  vs.  $k_z$  for this case as shown in Fig. 5. Peaks at  $k_z = q = 35.8\sqrt{\hbar m\omega_z}$  are clearly seen for  $\omega = 3807 \text{ s}^{-1}$  and these peaks fall within the tail of the oscillatory structures associated with the broadened  $k_z = 0$  condensate. These structures at  $k_z = q$  are responsible for the peaks in the spectral distribution in Fig. 4. The peak near  $\omega = 860 \text{ s}^{-1}$  and the minimum near  $\omega = 1636 \text{ s}^{-1}$  in Fig. 4 result due to subtle interference of the  $k_z = q$  peak with the structure surrounding the central ( $k_z = 0$ ) peak in Fig. 5. This kind of interference can occur when  $q$  (angle  $\theta$ ) is sufficiently small that the peak at  $k_z = q$  is within the structure of the central peak. It does not occur at  $\theta = 22.5^\circ$  ( $q = 0.390 \hbar k_{ph}$ ), rather only for angles  $\theta \leq 10^\circ$ .

In Fig. 6 we plot  $P_z$  versus  $\omega$  for  $\theta = 5^\circ$  ( $q = 8.72 \times 10^{-2} \hbar k_{ph} = 18\sqrt{\hbar m\omega_z}$ ),  $t_p = 6 \text{ ms}$  and potential well depths  $V_0 = 0.00162, 0.0054, 0.0162$  and  $0.054 E_R$ . At ultralow, low and intermediate intensities, an additional peak appears at  $\omega \approx 400 \text{ s}^{-1}$ . At all but ultralow intensity, the main peak in the spectrum is near the Bogoliubov frequency  $\Omega_B(q) = 2061 \text{ s}^{-1}$ . At ultralow intensity the peak at  $\omega \approx 400 \text{ s}^{-1}$  is even larger than that at  $\omega \approx 2000 \text{ s}^{-1}$  and  $P_z$  between these peaks becomes negative. Again, interference effects arising for reasons explained in connection with Fig. 5 are apparently responsible. A complicated interference pattern appears around the values of  $k_z = \pm q$  in  $|\psi(k_z, t)|^2$  vs.  $k_z$  (figure not shown). This interference plays a role in the determination of the spectrum shown in Fig. 6. The peaks in  $|\psi(k_z)|^2$  at  $k_z = q$  for  $\omega = 370$  and  $1687 \text{ s}^{-1}$  are larger than the peak at  $k_z = q$  for  $\omega = 990 \text{ s}^{-1}$ , and therefore maxima occur in the distribution shown in Fig. 6 at  $\omega = 370$  and  $1687 \text{ s}^{-1}$  and a minimum between the peaks in the spectrum occurs for  $\omega = 990 \text{ s}^{-1}$ .

Fig. 7 shows  $P_z$  versus  $\omega$  for  $\theta = 3^\circ$  ( $q = 5.24 \times 10^{-2} \hbar k_{ph} = 11\sqrt{\hbar m\omega_z}$ ),  $t_p = 6 \text{ ms}$  and  $V_0 = 0.00162, 0.0054, 0.0162$  and  $0.054 E_R$ . The peak near  $\omega = \Omega_B(q) = 1234 \text{ s}^{-1}$  for intermediate and high intensities becomes broadened at low intensity and then splits into two peaks at  $\omega \approx 400$  and  $1500 \text{ s}^{-1}$  for ultralow intensity, with the one at  $\omega \approx 400 \text{ s}^{-1}$  is about four times larger in magnitude than the one at  $\omega \approx 1500 \text{ s}^{-1}$ . The dip between the two peaks for the ultralow intensity is apparently also an interference effect that can not be explained in terms of a local density approximation to the Bogoliubov spectrum. For intermediate and high intensities, the peaks in  $|\psi(k_z)|^2$  at  $k_z = q$  are sufficiently large that interference with the structure around the  $k_z = 0$  peak does not occur and therefore the interference dip is absent.

#### IV. SUMMARY AND CONCLUSIONS

For very low optical intensities, long pulse duration and sufficiently large values of the momentum-transfer imparted by the light-potential, the local density approximation for the Bogoliubov excitation spectrum is a reasonable first approximation; the response peaks in  $P_z(q, \omega, V_0, t_p)$  versus  $\omega$  are broadened, particularly to lower values of  $\omega$ . However, we have shown that even for relatively low optical intensities, power broadening results and higher order processes occur that correspond to moving the atoms from the wave packet with central momentum  $k_z = q$  to wavepackets with central momentum  $2q$  and  $0$  as well as additional  $k_z = nq$ , with  $n > 2$  and  $n \leq -1$ . Moreover, at lower values of momentum-transfer  $q$  (smaller angles  $\theta$ ) where the wavelength of the optical potential becomes comparable to or larger than the size of the condensate, interference effects play a role in the dynamics, and directly affect the spectrum,  $P_z(q, \omega, V_0, t_p)$  versus  $\omega$  and can produce additional maxima and minima in the spectrum. The power spectrum of the order parameter after the optical potential is dropped,  $|\psi(k_z, t_p)|^2$  versus  $k_z$ , can be used to understand the nature of the spectra  $P_z(q, \omega, V_0, t_p)$  versus  $\omega$  and  $q$ .

One should keep in mind that the study performed here is a 1D calculation of the full 3D dynamics; 3D effects may modify details of the results we obtained. Nevertheless, we believe that the qualitative features of the conclusions will not change. We have detailed elsewhere how our quasi-1D calculations of the type we presented here model 3D aspects of the dynamics in cylindrically symmetric potentials [21], but this method can not describe radial excitations of the BEC that might arise due to the optical potential via the mean-field interaction. To the extent that radial excitations are not important, our method should be an adequate approximation to the 3D dynamics.

#### ACKNOWLEDGMENTS

We are extremely grateful to the group of Nir Davidson at Weizmann for sharing information about their experiments and for useful discussions. This work was supported in part by grants from the U.S.-Israel Binational Science

- 
- [1] M. R. Andrews *et al.*, Science 275, **637** (1997).  
 [2] E. W. Hagley *et al.*, Phys. Rev. Lett. **83**, 3112 (1999); M. Trippenbach, *et al.* J. Phys. B **33**, 47-54 (2000).  
 [3] B. P. Anderson and M. A. Kasevich, Science **282**, 1686 (1998).  
 [4] C. Orzel *et al.*, Science **291**, 2386 (2001).  
 [5] F. S. Cataliotti *et al.*, Science **293**, 843 (2001).  
 [6] J. Stenger *et al.*, Phys. Rev. Lett. **82**, 4569 (1999).  
 [7] D.M. Stamper-Kurn *et al.*, Phys. Rev. Lett. **83**, 2876 (1999).  
 [8] J.M. Vogels *et al.*, Phys. Rev. Lett. **88**, 060402 (2002).  
 [9] J. Steinhauer, R. Ozeri, N. Katz, and N. Davidson, Phys. Rev. Lett. **88**, 120407 (2002); cond-mat/0111438.  
 [10] R. Ozeri *et al.*, Phys. Rev. Lett. **88**, 220401 (2002).  
 [11] Ph. Nozières and D. Pines, *The Theory of Quantum Liquids* (Perseus Book, Cambridge, Massachusetts, 1999).  
 [12] N.N. Bogoliubov, J. Phys. U.S.S.R. **11**, 23 (1947); S.T. Beliaev, Sov. Phys.-JETP **7**, 289 (1958).  
 [13] D.S. Jin *et al.*, Phys. Rev. Lett. **77**, 420 (1996).  
 [14] M.O. Mewes *et al.*, Phys. Rev. Lett. **77**, 988 (1996).  
 [15] E.P. Gross, Nuovo Cimento **20**, 454 (1961); J. Math. Phys. **4**, 195 (1963).  
 [16] L.P. Pitaevskii, Zh. Eksp. Teor. Fiz. **40**, 646 (1961); Sov. Phys. JETP **13**, 451 (1961).  
 [17] Y.B. Band and M. Trippenbach, Phys. Rev. A **65**, 053602 (2002).  
 [18] A. Brunello *et al.*, cond-mat/0104051.  
 [19] M. Trippenbach, Y. B. Band, and P. S. Julienne, Phys. Rev. **A62**, 023608 (2000).  
 [20] M. Trippenbach, Y. B. Band, and P. S. Julienne, Optics Express **3**, 530 (1998).  
 [21] Y. B. Band, and I. Towers and B.A. Malomed, cond-mat/0207739.

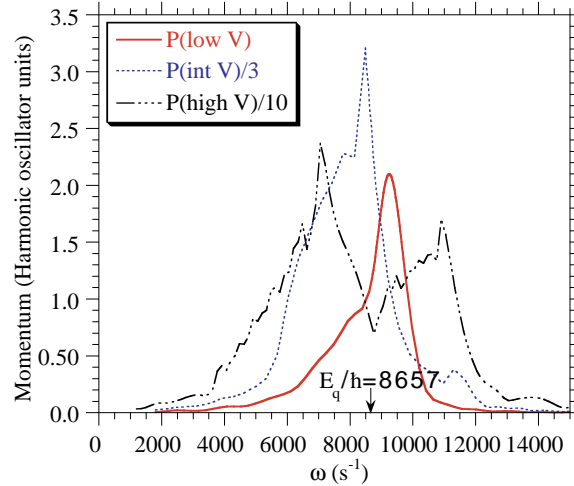


FIG. 1. Momentum  $P_z(q, \omega, V_0, t_p)$  versus  $\omega$  for  $\theta = 22.5^\circ$  ( $q = 0.390\hbar k_{ph}$ ) and pulse duration  $t_p = 6$  ms. Results for three different laser intensities corresponding to potential well depths  $V_0 = 0.0054$  (low),  $0.0162$  (intermediate) and  $0.054$  (high)  $E_R$  are shown.

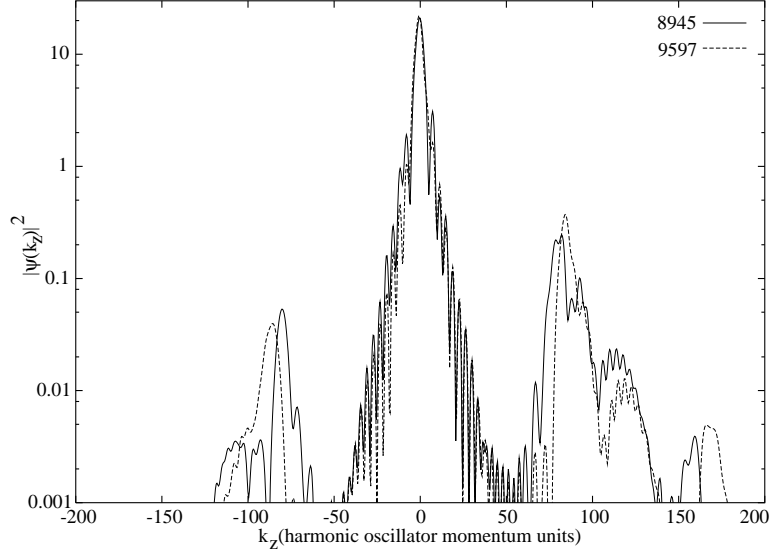


FIG. 2.  $|\psi(k_z, t)|^2$  vs.  $k_z$  for the low intensity case appearing in Fig. 1 at  $\omega = 8945$  and  $9597 \text{ s}^{-1}$ . The units of  $k_z$  are in harmonic oscillator momentum units  $\sqrt{\hbar m \omega_z} (= 2.44 \times 10^{-3} \hbar k_{ph})$ .

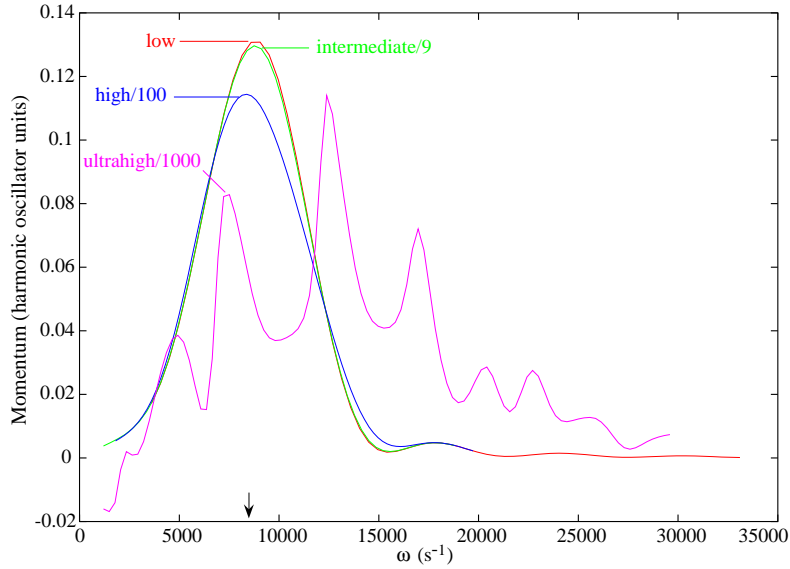


FIG. 3. Same as Fig. 1, except the pulse duration is 1 ms and an additional well depth of  $V_0 = 0.54$  (ultrahigh)  $E_R$  is included. The arrow indicates the position of  $\Omega_B(q)$ .

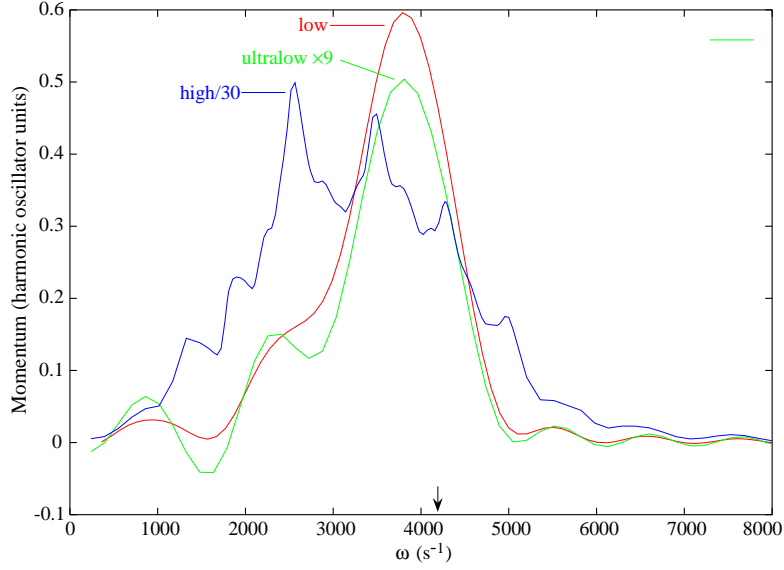


FIG. 4. Same as Fig. 1 except for  $10^\circ$  ( $q = 0.174 \hbar k_{ph}$ ). Results for three laser intensities corresponding to potential well depths  $V_0 = 0.00162, 0.0054$  and  $0.054 E_R$  are shown. The arrow indicates the position of  $\Omega_B(q)$ .

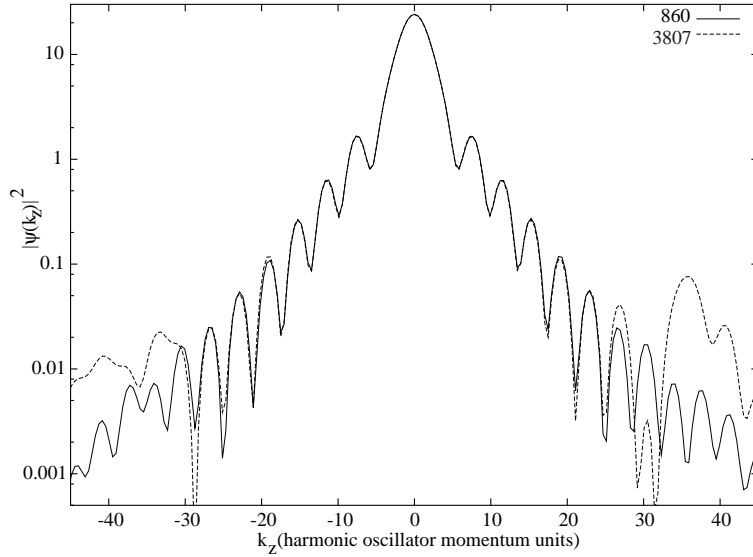


FIG. 5.  $|\psi(k_z, t)|^2$  vs.  $k_z$ , for the ultralow intensity case shown in Fig. 4 at  $\omega = 860$  and  $3807 \text{ s}^{-1}$ . The units of  $k_z$  are in harmonic oscillator momentum units  $\sqrt{\hbar m \omega_z} (= 2.44 \times 10^{-3} \hbar k_{ph})$ .

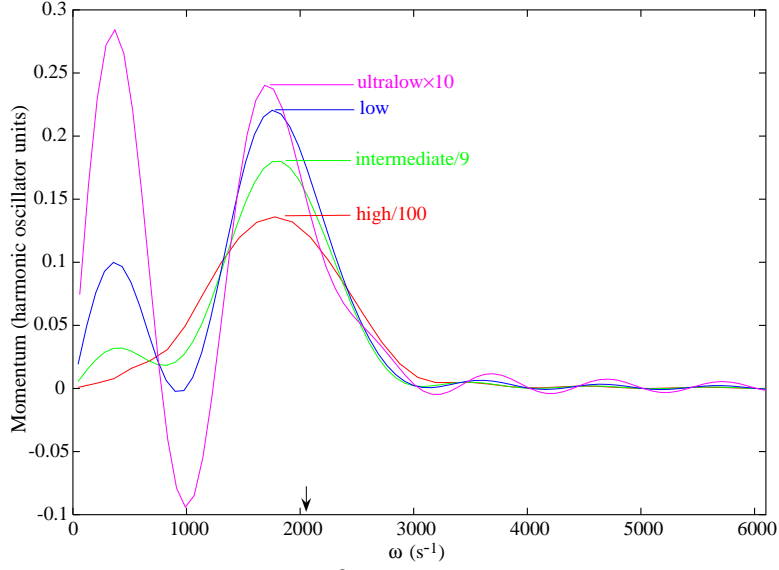


FIG. 6. Same as Fig. 1 except for  $5^\circ$  ( $q = 8.72 \times 10^{-2} \hbar k_{ph}$ ). Results for four different laser intensities corresponding to potential well depths  $V_0 = 0.00162, 0.0054, 0.0162$  and  $0.054 E_R$  are shown. The arrow indicates position of  $\Omega_B(q)$ .

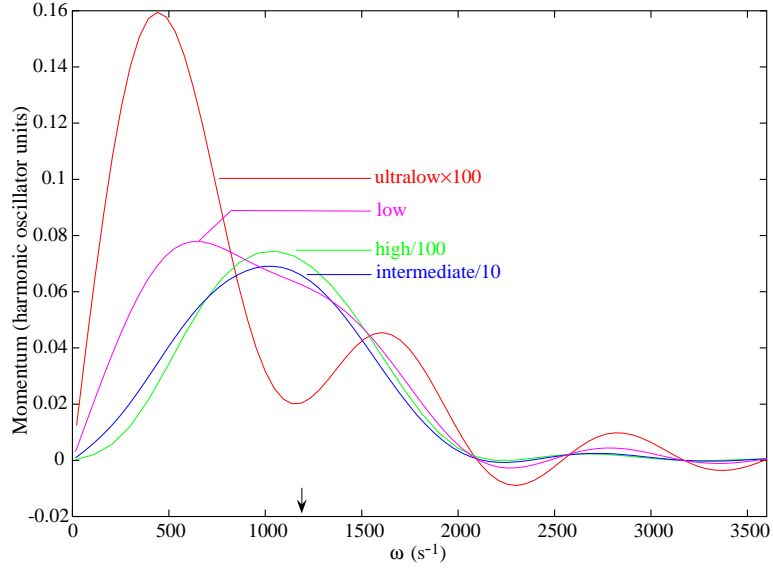


FIG. 7. Same as Fig. 1 except for  $3^\circ$  ( $q = 5.24 \times 10^{-2} \hbar k_{ph}$ ). Results for four different laser intensities corresponding to potential well depths  $V_0 = 0.00162, 0.0054, 0.0162$  and  $0.054 E_R$  are shown. The arrow indicates position of  $\Omega_B(q)$ .



